ASSESSMENT OF 2ND LEVEL INTERCONNECT QUALITY IN FLIP CHIP BALL GRID ARRAY (FCBGA) PACKAGE USING LASER ULTRASONIC INSPECTION TECHNIQUE

Vishnu V. B. Reddy, I. Charles Ume, Aaron M. Mebane
Georgia Institute of Technology
GA, USA
charles.ume@me.gatech.edu

Kola Akinade, Amiya R. Chaudhuri, Bryan Rogers, Cherif Guirguis, Kathy Derksen, Parimal Patel
MGMT-Quality, Cisco Systems, Inc.
GA, USA
akinadk@cisco.com

ABSTRACT

Flip chip packaging has a higher performance, and I/O density when compared with wire bonded packaging. However, wire bonding is extensively used in the electronic packaging industry. One of the difficulties with flip chip technology is testing its reliability. Advancements in Scanning Acoustic Microscopy (SAM) can provide insight into 1st level joint interconnects. However, these traditional solder joint inspection methods have been very unsatisfactory in assessing 2nd level interconnects because of the location and physical configuration of these solder joints. Non-destructive methods like SAM and X-Ray have their own limitations in assessment of 2nd level interconnects. The Laser Ultrasonic Inspection Technique uses laser pulses to generate bulk ultrasonic waves in the package, and the reflected waves from the 2nd level interconnect can give us information about the quality of the joint. A fiber-coupled laser interferometer is used to measure the transient out of plane displacements on the surface of the package. This is a direct measure of the reflected ultrasonic wave strength. Laser power can be adjusted depending on the size of the package to generate bulk waves of sufficient strength to reach the interconnections. In this project, Flip Chip Ball Grid Array (FCBGA) packages (foot print size 52.5mm x 52.5mm) from Cisco Systems were subjected to mechanical shock tests and analyzed using a Laser Ultrasonic Inspection (LUI) system. The results are validated using cross sectioning method. The samples are also tested using X-Ray and C-SAM, and the results are compared with those of the LUI system. The LUI system test results have demonstrated that the LUI method holds a great promise for assessing the presence of defects in 2nd level interconnects.

Key words: Laser Ultrasonic Inspection, Non-Destructive Method, Pad cratering, Inter Metallic Crack, Drop Test.

INTRODUCTION

Developments in Surface Mount Technology (SMT) have increased the density of solder joints, and levels of interconnects [1], making it more difficult to inspect microelectronic packages. Several competing non-destructive technologies, such as x-ray, and scanning acoustic microscopy (SAM) have been used to inspect underfill delamination and 1st level interconnects, that is the interconnections between the die and the package. However, most of these techniques have limitations in detecting defects in 2nd level interconnects, which are the interconnection between the package and the board. Figure 1 shows a schematic of an FCBGA package with 1st level and 2nd level solder ball interconnections [2].

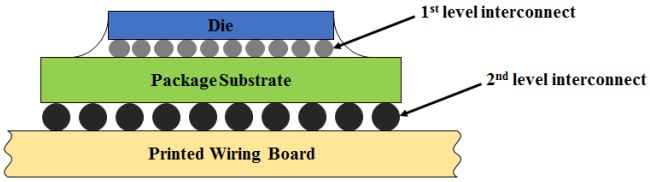

Figure 1. Configuration of FCBGA package

Though destructive methods like cross-sectioning and dye & pry can provide accurate results, they are time consuming, tedious, require sophisticated sample preparation and result in loss of the device. Also, there is a possibility that the failure signature itself might be lost during sample preparation. Hence, a reliable non-destructive technique for failure analysis of microelectronic packaging is in high demand in the semiconductor industry.

Semiconductor companies prefer SAM for quality control and failure analysis of microelectronics because it is a quick, safe and cheap non-destructive method that is currently available [3]. SAM is highly sensitive to the presence of air gaps, which makes it a popular method to detect delamination, voids and cracks in die, underfill, and 1st level interconnections (die solder bumps) [4]. However, acoustic microscopy has limitations in detecting defects in 2nd level interconnections (BGA solder balls). The die and the substrate are multilayer components. Incident acoustic energy is reflected at each interface, and thus acoustic energy will not suffice at the 2nd level interconnections to detect the presence of defects like pad cratering and Inter-Metallic Cracks (IMC). Water has to be used as a coupling

medium in SAM, and water could damage or affect the integrity of the package during inspection. Therefore, it is not considered as a fool-proof, non-destructive method of inspecting an electronic package.

X-Ray imaging is another popular non-destructive method of inspection for failure analysis of electronic packaging. In the 2D X-ray method, the test sample is irradiated using X-rays, and the interior structures of the test sample are imaged as a 2D projection. As this is a 2D projection of a 3D sample, internal failure regions may remain hidden. Hence, this technique does not reveal the true internal structure. Recent developments such as 3D X-ray microscopy (XRM) uses 2D images to reconstruct 3D tomographic slices using mathematical algorithms [5]. An XRM image clearly displays the internal structures. However, 2D images of high resolution and high quality are essential to show micro-cracks. Additionally, 3D X-ray is expensive technique.

Laser ultrasonic inspection (LUI) technique is a unique non-contact and non-destructive technique which can detect anomalies in the die, solder bumps, substrate and 2nd level interconnections. In this technique, ultrasound is generated in the package using a pulsed laser. The laser power is adjusted to retain the laser incident area within thermo-elastic regime to prevent any damage to the package. The transient out-of-plane displacement on the package surface due to laser ultrasound is measured by a laser interferometer. The presence of any anomaly at the solder ball will change the boundary condition or stiffness of the package, therefore altering the transient out-of-plane displacement response. Then the solder ball quality is assessed by correlating the measured displacement response of a known good reference sample to the response of the sample under inspection.

The LUI system has been successfully proven to detect missing solder bumps, cracks, non-wetting defects in solder bumps, voids, and micro cracks in solder balls of Plastic Ball Grid Array (PBGA) packages etc.[6][7][8]. In this paper, the capabilities of the LUI technique were demonstrated in assessing the 2nd level interconnect quality of FCBGA 52.5x52.5mm packages on a daisy chain test board. LUI was able to predict the failures in BGA solder balls caused by drop tests of the test board. Failures predicted by LUI are validated by cross sectioning the package, and analyzing cross section images using scanning electron microscopy (SEM). Further, finite element method (FEM) simulations were also carried out to confirm the potential failure sites during the drop tests.

LUI SYSTEM

Ultrasound generation and measurement

In SAM, ultrasound is generated by an external transducer and directed into the sample. Unlike in SAM, ultrasound is generated inside the test sample by localized heating of sample surface with a pulsed laser in LUI technique. The laser power is set high enough to generate good strength ultrasound, and low enough to avoid causing damage to the incident surface. Typically, the laser uses a 4-5ns pulse width. The temperature on the surface of the sample reaches a maximum, and drops quickly within 40-50ns time. The laser settings are adjusted such that ultrasonic waves are generated only in the thermo-elastic regime. Typical temperature profiles on a silicon die at various depths, with laser power of 80mW, and with laser pulse duration of 5ns are shown in Figure 2 [9].

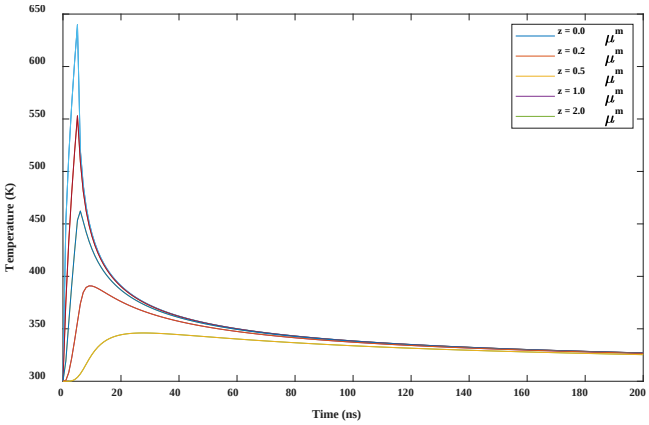

Figure 2. Temperature profile on the surface of silicon in response to an incident laser pulse

The temperature profile T(t), due to absorption of a laser pulse at the surface, is derived using Eq. 1 [9].

$$T(t) = \frac{2I_0(\kappa t)^{1/2}}{\sqrt{\pi}K} \qquad \text{(Eq. 1)}$$

where I_0 – absorbed laser flux density
K – Thermal conductivity
κ – Thermal Diffusivity
t – Time

$$I_0 = \frac{E_0}{At_0} = \frac{Absorbed\ laser\ energy}{Laser\ Spot\ Area}$$

The laser spot area used in this research is ~6.14mm^2. The absorbed laser energy E_0= (1-R)E, where E is the incident laser energy, and R is reflectivity. The reflectivity of photons at a wavelength of 1064nm for silicon is 0.43 at the incidence angle of 45°. The temperature profile as given in Figure 2 can be derived upon substituting all the values in Eq. 1. Analytically, the maximum temperature attained on the surface of the sample is around 640K, and it quickly cooled down to below 350K within 50ns. Thus, this temperature profile will not cause any damage to the incident surface.

A schematic of ultrasound generation and out-of-plane displacement measurement with an interferometer is shown in Figure 3. Localized heating produced by the laser generates thermo-elastic stresses, which in turn generate ultrasonic elastic waves that propagate deep within the sample [9]. Bulk ultrasound propagation and reflections

from the interfaces within a package are dependent on the material properties and internal structure of the package, including defects, solder ball joints, etc. The response of the ultrasound in the sample is detected by transient out-of-plane displacement measurement on the surface of the sample using a laser interferometer. Thus, transient out-of-plane displacement represents ultrasound propagation inside the sample.

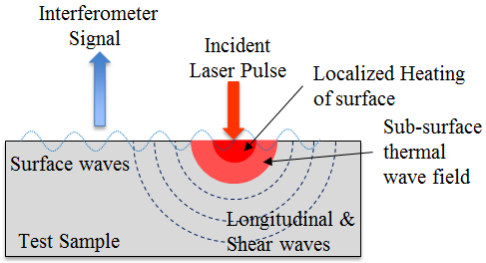

Figure 3. Ultrasound generation by Laser and measurement of transient out-of-plane displacement by interferometer

System setup

The LUI system consists of 1) a laser generator, 2) a multiplexer to split the beam into two, 3) two fiber optic cables with input and output couplers to deliver the laser on to the sample, 4) a laser interferometer, 5) an autofocus stage to move the interferometer towards and away from the sample to maximize the collected light, 6) a vision camera to locate the position and orientation of the sample on the fixture, and 7) positioning XY motion stages for the laser and the sample [10]. A photograph of the LUI system used is shown in Figure 4. The LUI system also consists of a vibrometer, a low pass filter, and a data acquisition controller to process, record and analyze the interferometer signal. The sample is held on the stage by vacuum to prevent movement during the inspection process.

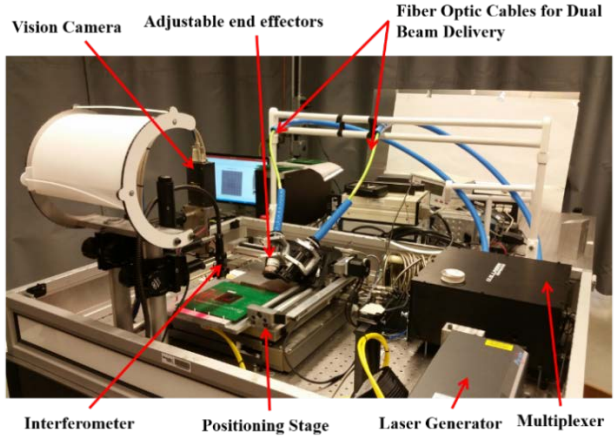

Figure 4. Schematic of LUI system setup

Signal analysis

The fiber optic laser interferometer is used to measure the out-of-plane surface displacement response at selected detection points. The principle of the laser ultrasound inspection system is to compare the surface displacement response of a known good reference package to that of the test package that is being inspected. Any anomaly near a detection point in the test package will produce a displacement response different from that of the response at the same detection point in the reference sample with no anomaly. Minor differences in the displacement response may arise from measurement instruments or environmental variations, although there are no considerable defects in the sample. To quantify the differences in displacement responses, a modified correlation coefficient (MCC) was used to analyze the interferometer signals. The MCC is given by the equation Eq. 2, as a correlation between the signals from the test sample and the reference sample at a detection point [6][7][8].

$$MCC = 1 - \left(\frac{\sum_n (R_n - \bar{R})(A_n - \bar{A})}{\sqrt{(\sum_n (R_n - \bar{R})^2)(\sum (A_n - \bar{A})^2)}} \right)^2 \quad \text{(Eq. 2)}$$

$$where \begin{cases} R_n: Reference\ signal & \bar{R}: Mean\ of\ R_n \\ A_n: Test\ sample\ signal & \bar{A}: Mean\ of\ A_n \\ n: \#of\ sampling\ points\ of\ the\ signal \end{cases}$$

From equation Eq. 2, MCC takes value between '0 and 1'. An MCC value of 0 indicates that the test signal and the reference signal match perfectly, indicating that there is no anomaly or defect. Similarly, an MCC value above a certain threshold value indicates an anomaly at that detection point.

TEST VEHICLES

Cisco Systems supplied test vehicles, as shown in Figure 5, which are subjected to drop tests as part of accelerated life testing. The test vehicle is a FCBGA package assembled on to a PWB of size 180mm x 180mm. FCBGA package contains a flip chip die of size 18.5mm x 20mm, underfilling, substrate of size 52.5mm x 52.5mm, and a total of 2597 BGA solder balls of each 0.5/0.6mm diameter at a pitch of 1mm arranged in 51 x 51 area array. As listed in Table 1, two test vehicles were inspected and are reported in this paper. One board (Board # 123) is used as a reference sample which did not undergo any testing.

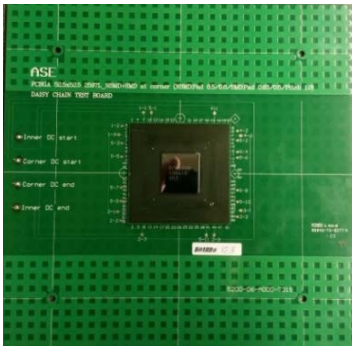

Figure 5. Test vehicle with FCBGA package

Table 1. Details of test vehicles and drop test conditions

Board Identification #	Drop Test Condition
123	Reference Board
83	150G pass; failed after 2 –z cycles of 200G
41	200G; 3 +z drop cycles; corner fail

Drop Test

The drop test is a popular accelerated life testing for the design of impact-tolerant electronic packages. The test vehicles used for this research are subjected to a board level reliability (BLR) drop test, which is a mechanical shock stressing of a package mounted to a PWB. The JEDEC standard, JESD22-B111 methodology, and service condition D is adopted in performing the BLR drop test [11]. Figure 6 shows a schematic illustration of the drop test set-up. Drop tests were conducted using a Lansmont M23 TTSII shock test system.

The drop table in Figure 6 is lifted, and released from a certain height. When the drop table is released, it travels down on guide rods, and strikes the strike surface, which is mounted over the rigid base. A base plate with standoffs is rigidly mounted on the drop table. The test vehicle assembly is mounted to the base plate standoffs using 4 shoulder screws at four corners. A stand-off distance of 10 mm is maintained between the PWB and the drop table in drop test experiments. The test vehicle is mounted on the base plate in two orientations as shown in the Figure 6, +Z orientation is when FCBGA package is facing upwards, and –Z orientation is when FCBGA package is facing downwards. An accelerometer is mounted on the PWB to measure the acceleration when the drop table strikes the strike surface. A typical impact pulse of drop test resembles a half sine wave as shown in Figure 7. Impact pulse generated in the test board during the drop measured at the center of the PWB is also shown in Figure 7. Drop tests were repeated with +Z and –Z orientations as given in Table 1 until failure of package occurred. Failure is detected by monitoring electrical continuity in the daisy chain. A 20% increase in resistance value in the daisy chain is considered as a failure.

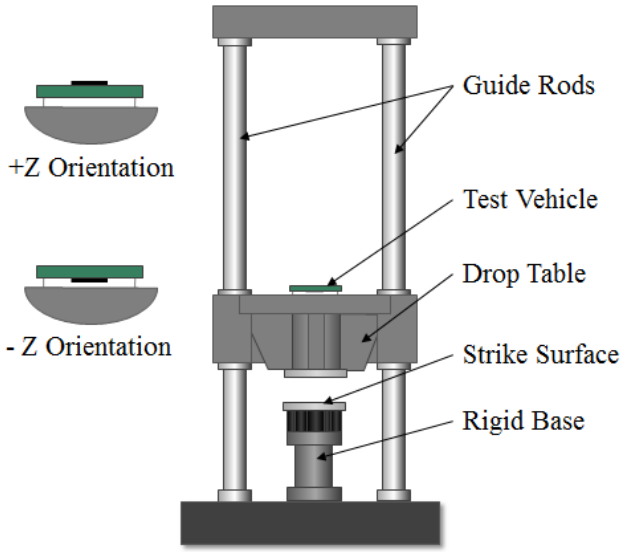

Figure 6. Drop Test Setup

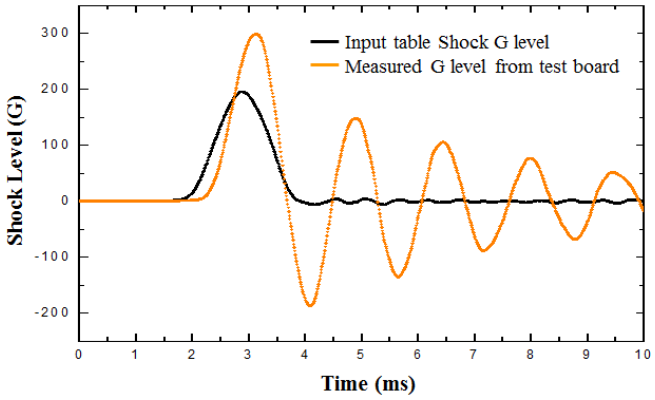

Figure 7. Input and measured shock G level

Inspection Pattern

High strength ultrasound and proximity of the inspection point to the defect are two key elements in detecting a defect in the LUI method. Ultrasound signal intensity is maximum at the laser incident point and attenuates with distance away from the incident point. Soft materials, multiple interfaces, and uneven geometry make the signal attenuate faster and at shorter distances. The package under discussion is a large package with soft underfill, and an 11- layered substrate. In order to receive a good interferometer signal (high amplitude signal), two options can be considered: 1) using very high power laser and making it incident at the center of the package and on top of the die, 2) dividing the package virtually into 9 sections, as shown in Figure 8, and making the low power laser to incident at the center of each section while collecting interferometer signal at inspection points in that section. The power of the laser that can be delivered to the package is limited by the power-carrying capacity of the optical fiber and the thermo-elastic temperature limit of the incident surface. Therefore, option 2 of dividing the package into 9 sections was selected in this research.

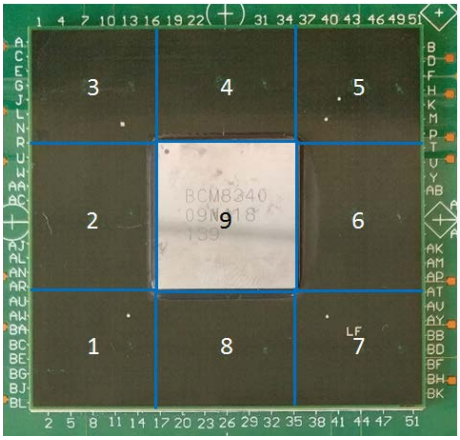

Figure 8. Virtual sub-division of the FCBGA package into 9 sections (Section 9 is dedicated to the die)

The package has 2597 BGA solder balls in total. Ideally, the interferometer data/signal should be collected at each location of BGA solder ball to determine its quality. However, the total inspection time depends on the number of inspection points. To reduce inspection time, an

inspection point is chosen for every 3x3 array of BGA solder balls. It is assumed that a defect or anomaly at any solder ball in the 3x3 array can affect the interferometer signal at that inspection point. The inspection pattern for section 5 is shown in Figure 9. Figure 9 is the X-ray image of the package with the inspection pattern superimposed on it. The black circles are BGA solder balls, blue spots correspond to inspection points, and red squares correspond to the 3x3 array of BGA solder balls that each inspection point targeted.

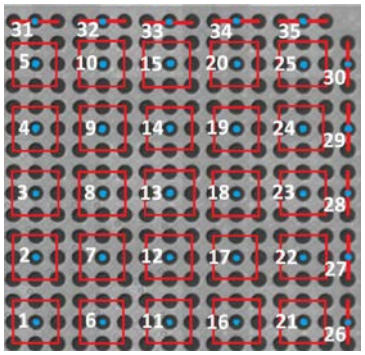

Figure 9. Inspection pattern of the section 5, superimposed on to the X-ray image of the chip package

LUI TEST RESULTS

Two test vehicles and a reference board as listed in Table 1 were examined using LUI test. Laser power of 80mW (total power) was used for these boards for testing. Other system parameters are listed in Table 2. Initially, interferometer transient out-of-plane displacement signals were collected on the reference board (#123), and then on the test vehicles based on the inspection pattern described in the previous section. MCC values are calculated using equation Eq. 2 at each inspection point, and plotted in the form of a 3D histogram. LUI results (MCC values) for board # 83 are shown in Figure 10, and for board # 41 are shown in Figure 11.

Table 2. Parameters used in LUI system for evaluation of test vehicles

Total pulsed laser power	80 mW
Laser wavelength	1064 nm
Pulse length	5ns
Pulse frequency	20 Hz
Interferometer sampling rate	50 MS/Sec
# of sample points considered for MCC	3000
# of signals average per inspection point	128

The general observation is that MCC values are low at most of the inspection points. This indicates minor or no difference in the test package when compared with the reference package (board # 123). In both test packages, the corner MCC values are high, indicating defects at the corners. Even, from the Finite Element Method (FEM) analysis, corner solder balls are expected to fail in the drop test. Hence, it is predicted that the corner solder balls will have failures. Apart from the corners, there were observed to be high MCC values in section 2 and section 6 for board # 41. These high MCC values are attributed to noise in the interferometer signals because of the rough and uneven surface of the package in that specific area.

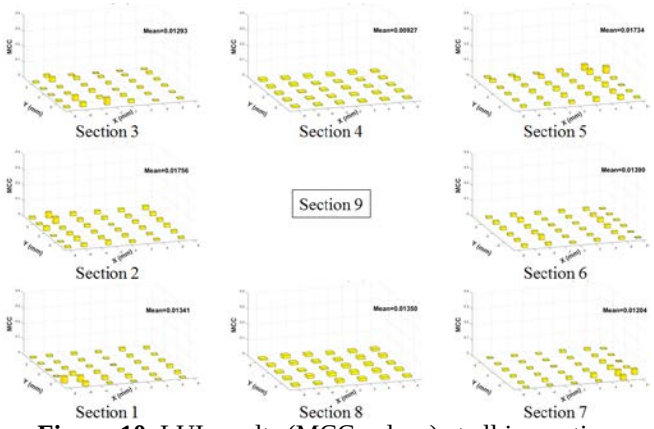

Figure 10. LUI results (MCC values) at all inspection points for board # 83 in 3D histogram format

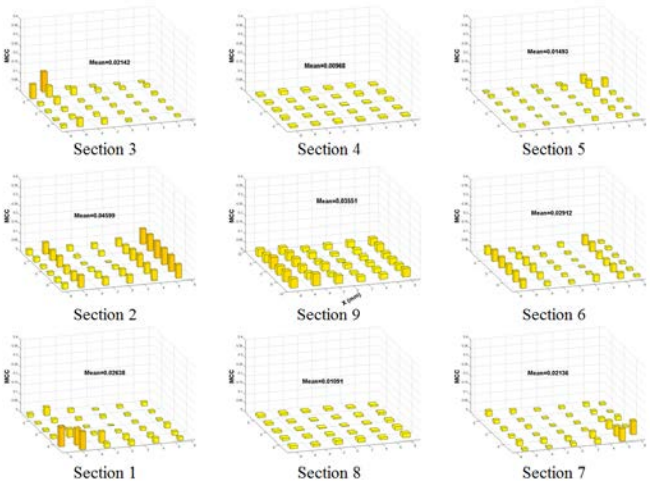

Figure 11. LUI results (MCC values) at all inspection points for board # 41 in 3D histogram format

FINITE ELEMENT METHOD SIMULATIONS

FEM with a three dimensional quarter model, as shown in Figure 12 was developed to understand the failure trends in BGA solder balls and to validate the LUI results. The FEM model consists of five components, silicon die, underfill, substrate, BGA solder balls, and PWB, as shown in Figure 13.

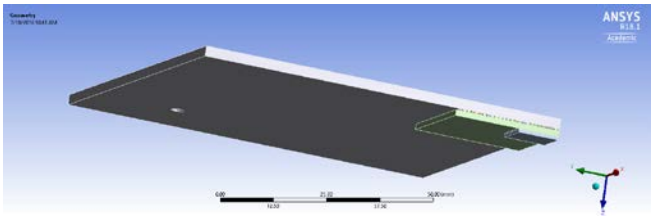

Figure 12. Three dimensional 1/4th model of FCBGA package mounted on PWB

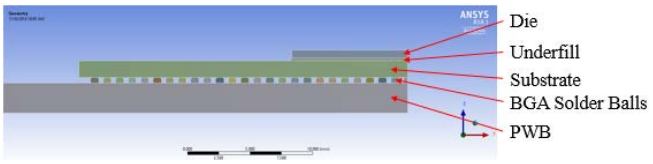

Figure 13. FEM model of test vehicle showing different components

During actual drop tests, the pulse generated on the drop table is transferred to the PWB through the four corner screws. Hence, the impact pulse measured in the experiment can be given as input to the FEM model of only the PWB with a package mounted on it. In this way, all other drop test apparatus can be eliminated completely from the FEM model. The input table shock G level and measured G level at the center of the test board are shown in Figure 7. From the experiments, and strain measurement, it is clear that the PWB has maximum deflection, and maximum strain at the center for the given shock pulse [12]. The measured G level is supposed to be applied at the center of the board (on the other side of the package). However, ANSYS workbench does not support applying acceleration at a point in transient structural analysis. Therefore, harmonic acceleration is converted to displacement amplitude using Eq. 3, and the displacement is applied at the center of the board while the board was fixed at the corner hole (representing that the board is screwed to the drop table), and symmetric boundary conditions were applied on symmetric sections.

$$d = -\frac{a}{\omega^2} = -\frac{a}{(2\pi f)^2} \qquad \text{(Eq. 3)}$$

where d: displacement; a: acceleration;
ω: angular frequency; f: frequency.

The equivalent stress distribution results obtained from the FEM analysis are shown in Figure 14. It is observed that corner solder balls experience high stress. These corner solder balls are prone to failure on multiple drop or impact cycles. It should be noted that the LUI results also show high MCC values at the corner solder balls as shown in Figure 10 and Figure 11. Hence, FEM results are helpful in confirming high MCC values at the corner inspection points of the package, aligning with LUI results.

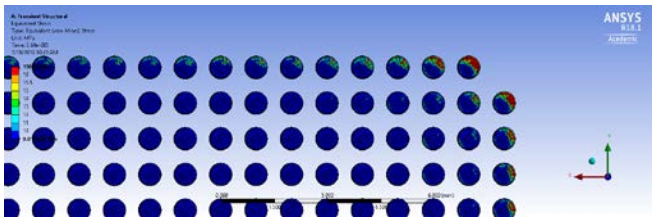

Figure 14. Equivalent stress distribution in the solder balls at interface between solder balls, and PWB

VALIDATION & DISCUSSION

From the FEM results and LUI results, it is estimated that the corner solder balls are failed. To validate the presence of failures, the test samples were cross sectioned, polished, and observed via scanning electron microscope (SEM). Board # 83 was cross sectioned along column 51 of solder balls, and board # 41 was cross sectioned along column 1 of solder balls. LUI test results along column 51 of solder balls for board # 83 were shown in Figure 15. LUI test results along column 1 of solder balls for board # 41 are shown in Figure 16. Figure 15, and Figure 16 show MCC values along the column of solder balls in the form of a 2D histogram.

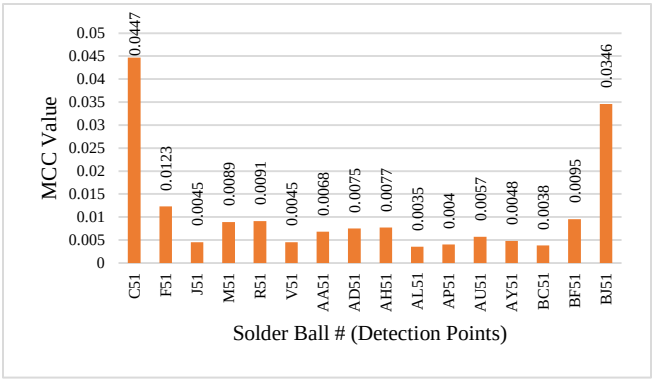

Figure 15. LUI results along the column 51 of solder balls for the board # 83

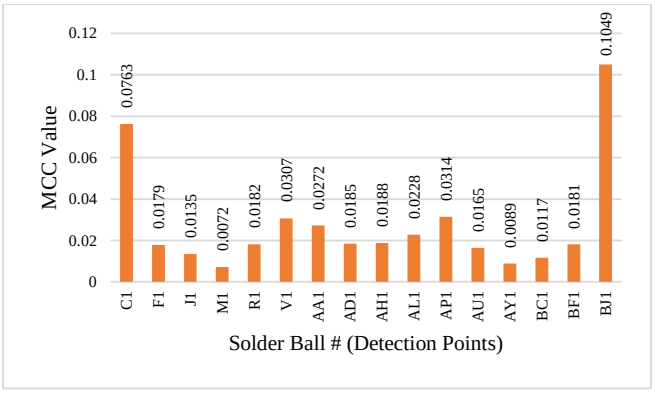

Figure 16. LUI results along the column 1 of solder balls for the board # 41

Figure 17 through Figure 23 show the cross-sectional SEM images of corner solder bumps of board # 83, and board # 41. Board # 83 was observed to have intermetallic cracks (IMC) in the corner balls, as shown in Figure 17 (solder ball B51), Figure 15 (solder ball C51), and Figure 19 (solder ball BK51). The MCC value corresponding to solder balls B51, and C51 is 0.0447 (at inspection point on C51), and the MCC value corresponding to solder balls BK51 is 0.0346 (at inspection point on BJ51). These MCC values are clearly higher than the MCC values at other inspection points in the same column. This confirms that high MCC values at the corners of the package for board # 83 correspond to IMCs in the solder balls (on PWB side). Also, the IMCs in two solder balls B51 and C51 at one corner produced high MCC values when compared to the IMC on only solder ball BK51 at the other corner. Thus, the cumulative severity of the defects is correlated with the level of MCC value.

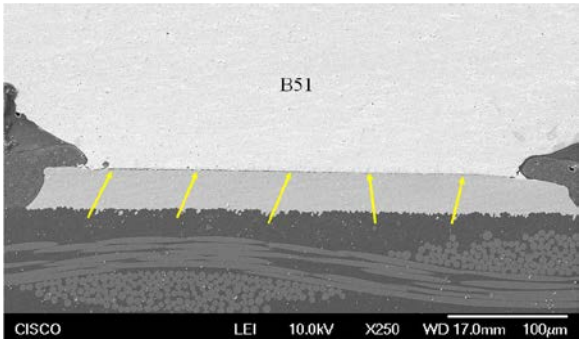

Figure 17. Crack in the intermetallic layer of the solder ball B51 in board # 83

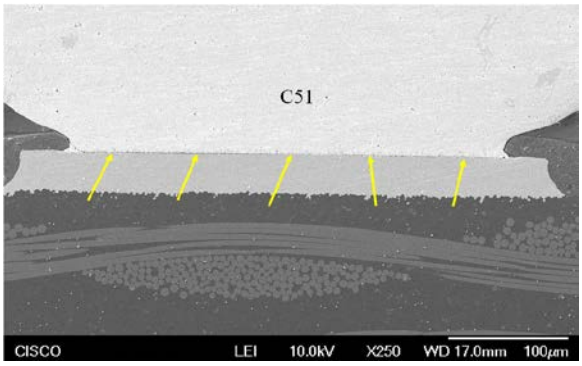

Figure 18. Crack in the intermetallic layer of the solder ball C51 in board # 83

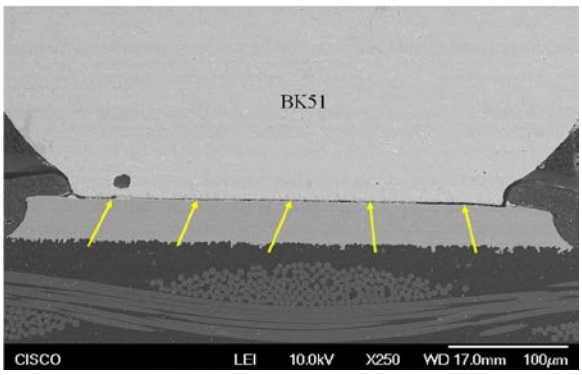

Figure 19. Crack in the intermetallic layer of the solder ball BK51 in board # 83

From the SEM images, Board # 41 was observed to have pad cratering in the PWB in corner solder balls as shown in Figure 20 (solder ball B1), Figure 21 (solder ball BH1), Figure 22 (solder ball BJ1), and Figure 23 (solder ball BK1). The MCC value corresponding to solder ball B1 is 0.0763 (at inspection point on C1), and the MCC value corresponding to solder balls BH1, BJ1 and BK1 is 0.1049. Again, the defects in three solder balls (BH1, BJ1 and BK1) resulted in high MCC values. Also, BK1 has worst case pad cratering. High MCC values in board # 41 correspond to a pad cratering defect unlike the IMC in board # 83. The failure modes of the two packages are different because the corner solder ball pads of board # 83 are solder mask defined, whereas all pads on board # 41 are non-solder mask defined.

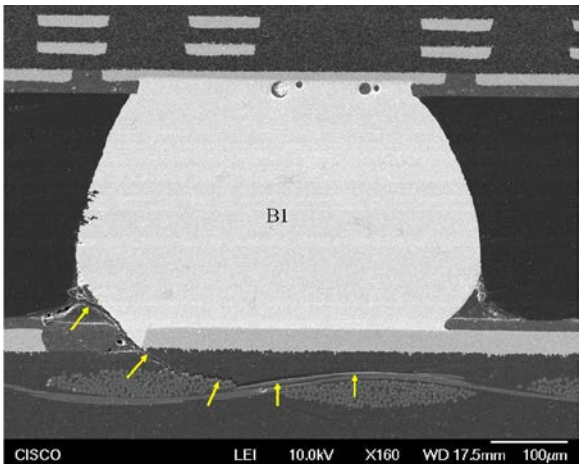

Figure 20. Partial pad cratering in the solder ball B1 in te board # 41

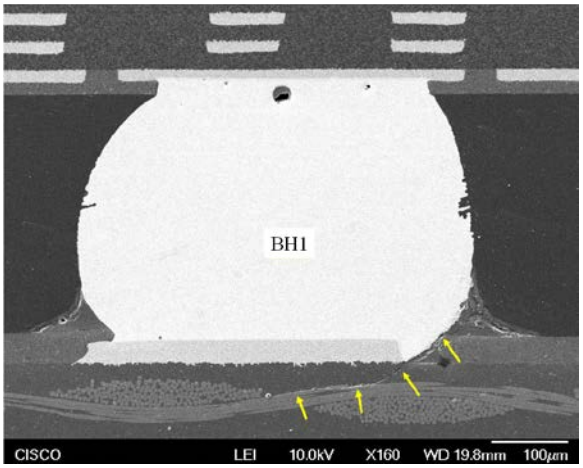

Figure 21. Partial pad cratering in the solder ball BH1 in board # 41

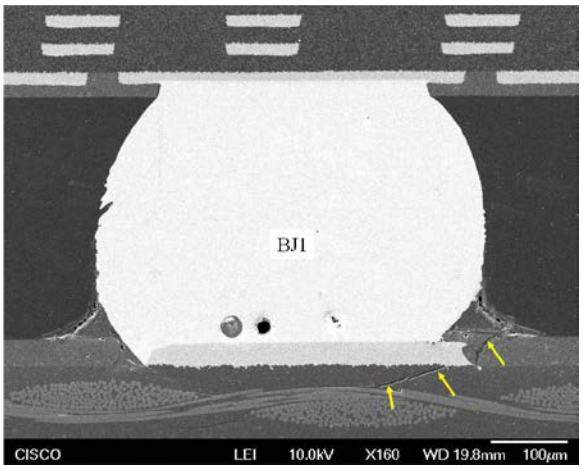

Figure 22. Partial pad cratering in the solder ball BJ1 in board # 41

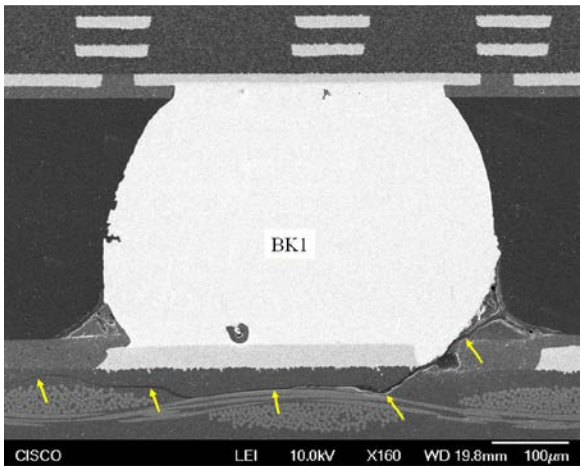

Figure 23. Partial pad cratering in the solder ball BK1 in board # 41

LUI results show that the corner solder balls of the packages that were subjected to shock testing have high MCC. The corner solder balls have been shown to have IMC and pad cratering defects from the cross-section SEM images. Thus, the LUI results are validated. Though a high MCC value corresponds to some defect or anomaly, it is difficult to predict the kind of defect with this system. A study of interferometer signals is being carried out to develop a method to differentiate various defects.

Acoustic microscopy (echo method), and X-Ray (2D) could not detect the presence of defects in 2nd level interconnects. Sample results from a FCBGA package that was analyzed using Acoustic microscopy with 200MHz transducer are shown in Figure 24. Acoustic waves were able to penetrate up to only one layer of substrate out of 11 layers. Figure 24 shows through holes between the top layer and the next layer. Even with low frequency ultrasound, it is very difficult to detect defects like IMC and pad cratering in solder balls.

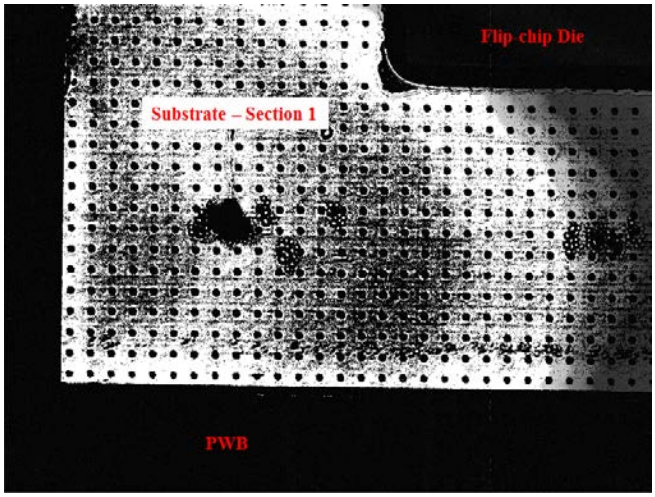

Figure 24. Sample results from scanning acoustic microscopy (SAM) with 200MHz transducer

Sample 2D X-ray results of an FCBGA package using a DAGE X-ray machine are shown in Figure 25. This image is a 2D projection of the sample. Minor cracks are hidden under voids and other structural constraints for X-rays in 2D projection. Hence, IMC and pad catering defects were not detected with the 2D X-ray technique. The 3D X-ray microscopy technique is gaining popularity in the modern era. However, high resolution 2D images are required to detect IMC and pad cratering defects with the 3D X-ray technique.

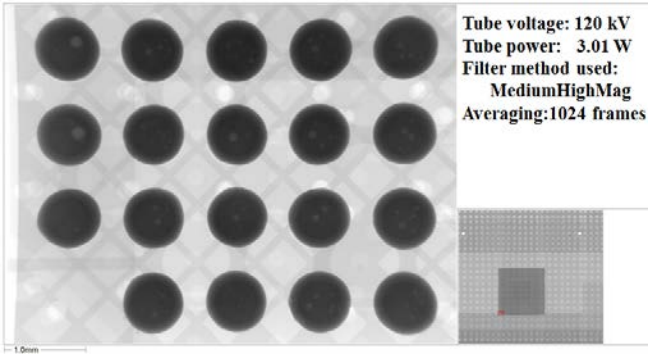

Figure 25. Sample X-ray image of a corner of FCBGA package from DAGE X-ray inspection system

CONCLUSION

Laser Ultrasonic inspection (LUI) is a unique and promising non-destructive inspection technique for assessing 2nd level interconnection quality, and determining the presence of BGA solder ball defects in FCBGA packages. Reasonable efforts have been made to detect 2nd level interconnect defects using acoustic microscopy, and 2D X-ray. It is concluded that only LUI can detect IMC and pad cratering defects. LUI results are validated with FEM and cross-sectional SEM images. The LUI system not only captures the general trend of 2nd level interconnection quality, but also estimates the defect severity by using MCC values. It is found that drop testing can induce pad cratering and IMC defects in test samples. Although the LUI technique could not distinguish the type of the defect, LUI could successfully detect minor cracks in 2nd level interconnections. Further efforts are in place to improve the sensitivity and resolution of the system by using high laser power to detect micro cracks in packages.

ACKNOWLEDGEMENT

The authors would like to thank Cisco Systems Inc., and the Manufacturing Machines and Equipment of the National Science Foundation (Grant Number 128866) for their financial support and valuable technical support.

REFERENCES

[1] Tummala, R.R., Fundamentals of microsystems packaging. 2001: McGraw-Hill.
[2] Flip Chip Ball Grid Array Package Reference Guide, Texas Instruments, Literature Number: SPRU811A, May 2005.

[3] L. Ma, S. Bao, D. Lv, Z. Du and S. Li, "Application of C-mode Scanning Acoustic Microscopy in Packaging," 2007 8th International Conference on Electronic Packaging Technology, Shanghai, 2007, pp. 1-6.
[4] J. E. Semmens and L. W. Kessler, "Characterization of flip chip interconnect failure modes using high frequency acoustic micro imaging with correlative analysis," 1997 IEEE International Reliability Physics Symposium Proceedings. 35th Annual, Denver, CO, USA, 1997, pp. 141-148.
[5] S. M. Zulkifli, B. Zee, W. Qiu and A. Gu, "High-res 3D X-ray microscopy for non-destructive failure analysis of chip-to-chip micro-bump interconnects in stacked die packages," 2017 IEEE 24th International Symposium on the Physical and Failure Analysis of Integrated Circuits (IPFA), Chengdu, 2017, pp. 1-5.
[6] J. Gong, and I. C. Ume, "Nondestructive Evaluation of Poor-Wetted Lead-Free Solder Bumps in Ball Grid Array Packages Using Laser Ultrasound, and Interferometric Technique," in IEEE Transactions on Components, Packaging, and Manufacturing Technology, vol. 3, no. 8, pp. 1301-1309, Aug. 2013.
[7] L. Zhang, I. C. Ume, J. Gamalski, and K. P. Galuschki, "Detection of flip chip solder joint cracks using correlation coefficient, and auto-comparison analyses of laser ultrasound signals," IEEE Trans. Compon. Packag. Technol., vol. 29, no. 1, pp. 13-19. March 2006.
[8] Gong, et al. Non-destructive Evaluation of Solder Ball Quality under Mechanical Bending Using Laser Ultrasonic Technique, SMTA Journal, Volume 28 Issue 3, 2015.
[9] Scruby, C. B., and Drain, L. E., Laser ultrasonics: techniques, and applications. Bristol: Adam Hilger, 1990.
[10] Aaron M. Mebane, Dr. I. C. Ume, Vishnu V. B. Reddy, and Kola Akinade, “Feasibility studies and Advantages of using Dual Fiber Array in Laser Ultrasonic Inspection of Electronic Chip Packages”, unpublished.
[11] JEDEC JESD 22-B111: Board Level Drop Test Method of Components for Handheld Electronic Products
[12] Q. Wang, W. Xie and M. Ahmad, "Experimentally validated analysis and parametric optimization of monotonic 4-point bend testing of advanced BGA packages," 2012 13th International Conference on Electronic Packaging Technology & High Density Packaging, Guilin, 2012, pp. 706-713.